Macromolecules

Article

Cite This: Macromolecules 2018, 51, 3017−3029

Competitive Hydrogen Bonding Interactions Influence the Secondary and Hierarchical Self-Assembled Structures of Polypeptide-Based Triblock Copolymers

Cheng-Chang Tsai,[†] Zhihua Gan,[‡] Tao Chen,[§] and Shiao-Wei Kuo*[,†,∥]

[†]Department of Materials and Optoelectronic Science, National Sun Yat-Sen University, Kaohsiung 80424, Taiwan

[‡]State Key Laboratory of Organic−Inorganic Composites, College of Life Science and Technology, Beijing University of Chemical Technology, Beijing 100029, China

[§]Ningbo Institute of Material Technology and Engineering, Chinese Academy of Science, Zhongguan West Road 1219, 315201 Ningbo, China

[∥]Department of Medicinal and Applied Chemistry, Kaohsiung Medical University, Kaohsiung, Taiwan

Supporting Information

ABSTRACT: A new biocompatible triblock copolymer, poly(ε-caprolactone-*b*-ethylene oxide-*b*-γ-benzyl L-glutamate) (PCL-*b*-PEO-*b*-PBLG), has been prepared through sequential ring-opening polymerizations, with two degrees of polymerization for the PBLG block segment when using an amino-terminated PCL-*b*-PEO diblock copolymer as the macroinitiator. The hydrogen bonding strengths (interassociation equilibrium constants) followed the order of phenolic/PEO (K_A = 264.8) > phenolic/PCL (K_C = 116.8) > phenolic/PBLG (K_D = 9.0), indicating that the phenolic OH groups preferred to interact with the C−O−C units of PEO block, then the C═O units of PCL block, and finally with the C═O units of PBLG block. The hydrogen bonding behavior of these four competing functional units could be predicted accurately using the Painter−Coleman association model. These competitive hydrogen bonding interactions induced various miscibility behaviors and self-assembled hierarchical structures, ranging from the hexagonally packed cylinder structure of α-helical conformation of PBLG block segment in the crystalline lamellar structure of the PCL block segment to a miscible ordered structure upon increasing phenolic concentrations in the phenolic/PCL-*b*-PEO-*b*-PBLG blend system.

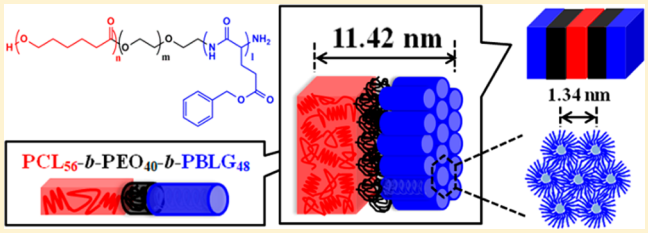

INTRODUCTION

Diblock copolymer/homopolymer blends having the form A-*b*-B/C, stabilized through hydrogen bonding where the homopolymer C interacts with either the A or B block segments, have been investigated widely in polymer science for their unusual self-assembled structures.[1−24] We have found that the hydrogen bonding strength, which can be characterized by the ratio of inter- and self-association equilibrium constants (K_A/K_B), is a key factor determining which self-assembled structure forms when the C homopolymer is miscible only with the B block segment (i.e., when C is immiscible with the A block segment).[5−7] We and Guo et al. have also proposed that different hydrogen bonding strengths (i.e., different values of K_A and K_C) lead to different composition-dependent self-assembled structures when the homopolymer C interacts with both A and B block segments.[8−15]

In addition to diblock copolymers, ABC triblock copolymers can also form self-assembled hierarchical structures—including three-phase lamellar structures, alternative spherical structures, and core/shell cylindrical structures—and have received much recent interest.[25−31] Unlike A-*b*-B/C blends, however, the blending of ABC triblock copolymers with homopolymers D, capable of competitive hydrogen bonding, has rarely been examined for their corresponding self-assembled structures and morphological transitions. For example, Guo et al. reported various composition-dependent self-assembled structures, including spherical, cylinder, and lamellar structures, in poly(ethylene oxide-*b*-4-vinylpyridine-*b*-styrene)/poly(vinylphenol) blends.[32] Other previous studies also employed poly(styrene-*b*-ethyl acrylate-*b*-ethylene oxide), poly(styrene-*b*-methyl methacrylate-*b*-ethylene oxide), poly(polystyrene-*b*-2-vinylpyridine-*b*-ethylene oxide), poly(ethylene−ethylene oxide-*b*-ε-caprolactone), and poly(ethylene oxide-*b*-styrene-*b*-isoprene) as templates blended with resol-type phenolic as a carbon source to obtain highly ordered mesoporous carbons.[33−43] Here, the phenolic or poly(vinylphenol) homopolymer (homopolymer D) only shows miscible with one or two block segments (e.g., P4VP, P2VP, PEO, PCL, PEMA, or PMMA block segments) through hydrogen bonding; however, it was immiscible with the PE, PI, or PS block segment.

Received: January 14, 2018
Revised: March 31, 2018
Published: April 6, 2018

DOI: 10.1021/acs.macromol.8b00087
Macromolecules 2018, 51, 3017−3029

Scheme 1. Synthesis of the (a) PCL-*b*-PEO-NH_2 Diblock Copolymer and (b) PCL-*b*-PEO-*b*-PBLG Triblock Copolymers

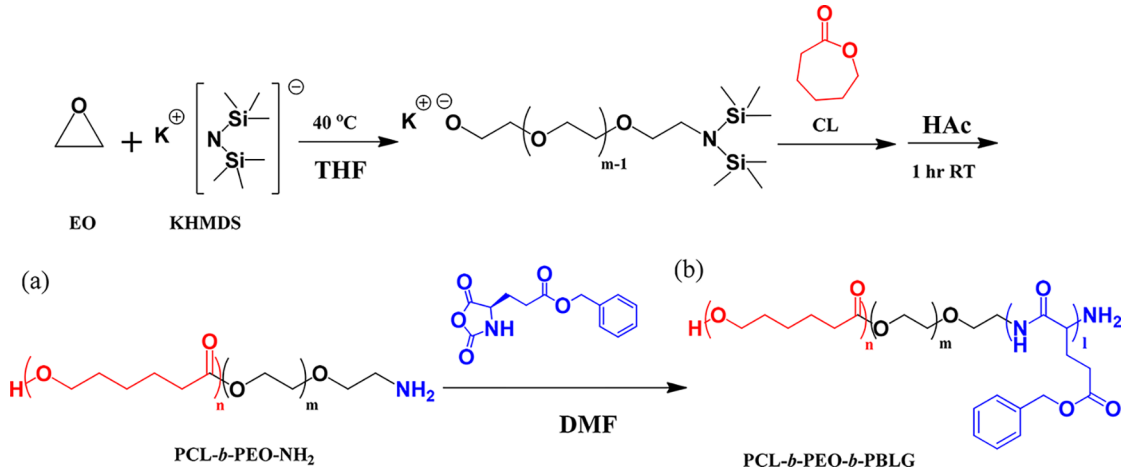

In this study, we synthesized new polypeptide-based poly(ε-caprolactone-*b*-ethylene oxide-*b*-γ-benzyl L-glutamate) (PCL-*b*-PEO-*b*-PBLG) triblock copolymers through sequential ring-opening polymerizations (ROPs; Scheme 1) and blended them with phenolic resin. The preparation of poly(non-peptide)-*b*-polypeptide block copolymers has potential applications in drug delivery or tissue engineering,[44−47] and these systems could provide the stabilization for α-helical conformation to pure PBLG homopolymer. This system possesses a new A-*b*-B-*b*-C/D blend type, where D is miscible with all of the A, B, and C block segments through strong intermolecular hydrogen bonding. Using the Painter−Coleman association model,[48] we have determined that the hydrogen bonding strengths (K_A) follow the order phenolic/PEO (K_A = 264.8)[49] > phenolic/PCL (K_C = 116.8)[50] > phenolic/PBLG (K_D = 9.0)[51] (Scheme 2), suggesting that the strongest hydrogen bonding of phenolic resin should exist with the B block, with relatively weaker interactions with the A and C blocks. Here, we need to emphasize that both PEO and PCL will interact with phenolic resin in a multivalent fashion through the main backbone, while only side chains interactions are involved in the case of PBLG.

Scheme 2. Interassociation Equilibrium Constants, Based on PCAM, for (A) Phenolic/PEO (K_A = 264.7), (B) Phenolic/PCL (K_C = 116.8), and (C) Phenolic/PBLG (K_D = 9.0) Blend Systems

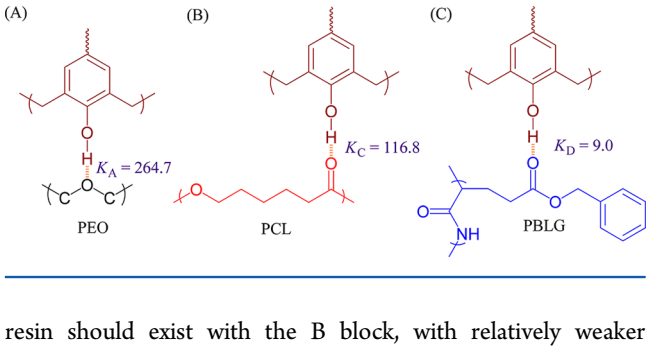

It has been previously shown that the main backbone of PBLG does not interact with phenolic resin as peptide bonds are strongly involved in intramolecular hydrogen bonding interactions, which are necessary for α-helix conformation.[51]

As a result, we expected that the phenolic OH groups prefer to interact with the PEO block segment at low phenolic contents, interact with both the PEO and PCL block segments at moderate phenolic contents, and interact with all PEO, PCL, and PBLG block segments at high phenolic contents. This paper describes the first example of predictable hydrogen bonding behavior of four competing functional units. The miscibility, self-assembly, and secondary structures formed in this phenolic/PCL-*b*-PEO-*b*-PBLG blend system, mediated by hydrogen bonding interactions, are discussed below in detail.

EXPERIMENTAL SECTION

Materials. Caprolactone monomer (Acros) was dried (CaH_2) and purified through vacuum distillation (70 °C); the ethylene oxide monomer (BDH Limited Poole) was dried (CaH_2) at 0 °C and then stored at −20 °C. L-Glutamic acid (99%), *tert*-butanol, trimethylamine, and triphosgene were purchased from Alfa Aesar. Benzyl alcohol, magnesium sulfate, and sodium bicarbonate were purchased from SHOWA. Ethyl acetate (EtOAc), methanol (MeOH), sulfuric acid (H_2SO_4), *N*,*N*-dimethylformamide (DMF), and ethanol (EtOH) were used as received. Novolac-type phenolic resin was prepared by H_2SO_4-catalyzed condensation, using a procedure described previously.[41]

PCL-*b*-PEO-NH_2 Diblock Copolymer.[52] The PCL-*b*-PEO-NH_2 diblock copolymer was prepared through sequential ROPs with $[(CH_3)_3Si]_2NK$ as an initiator, using a procedure described previously.[52] After polymerization of the PEO and PCL blocks, acetic acid was then introduced to terminate the ring-opening polymerization and also deprotect the amino unit. The solution was poured into the excess cold ether to precipitate the PCL-*b*-PEO-NH_2 diblock copolymer, which was collected and dried in the vacuum oven at room temperature overnight to obtain the pure white powder.

PCL-*b*-PEO-*b*-PBLG Triblock Copolymer. The triblock copolymer PCL-*b*-PEO-*b*-PBLG was prepared through ROP of BLG-NCA monomer with the PCL-*b*-PEO-NH_2 diblock copolymer as an macroinitiator. Desired amounts of the BLG-NCA monomer (0.51

Table 1. Characterization Data of the PCL-*b*-PEO-NH_2 Diblock Copolymer and the PCL-*b*-PEO-*b*-PBLG Triblock Copolymers

polymers	theor M_n (Da)	M_n (^{1}H NMR, Da)	M_n (GPC, Da)	yield (%)	PDI (GPC)	T_m (°C)
$CL_{56}EO_{40}$-NH_2	8100	8100	26300	85	1.22	49.6/53.4
$CL_{56}EO_{40}BLG_{20}$	9760	11400	38400	82	1.23	52.5
$CL_{56}EO_{40}BLG_{48}$	16400	16000	40500	79	1.34	54.2

DOI: 10.1021/acs.macromol.8b00087
Macromolecules 2018, 51, 3017−3029

g) and PCL-*b*-PEO-NH_2 (0.5 g) were placed in a silanized flask, which was connected to the vacuum line for 0.5 h. DMF (10 mL) was added via syringe. After stirring the solution for 24 h at 0 °C, the resulting triblock copolymer was precipitated in cold MeOH, redissolved in DMF, and recovered through precipitation in MeOH. The triblock copolymer was purified three times from CH_3OH/Et_2O to obtain pure white powder, which was dried under in an oven at 40 °C (yield: 79%). Table 1 summarizes the physical properties of the PCL-*b*-PEO-*b*-PBLG triblock copolymers.

Blend Preparation. Various blends of phenolic and PCL-*b*-PEO-*b*-PBLG (blend composition: 5 wt %) were prepared through solution-casting. The mixture was dissolved in DMF until the solutions become homogeneous. The solvent was evaporated at 40 °C for 24 h slowly and then under high vacuum at 100 °C for 72 h to ensure the removal of residual solvent.

Characterization. The molecular weights and polydispersity (PDI) of the PCL-*b*-PEO-*b*-PBLG triblock copolymers were measured through gel permeation chromatography (GPC) by using the Waters 510 HPLC with DMF as an eluent (flow rate: 1.0 mL/min). The calibration curves of these systems were constructed by using PS standards with the combination of UV and refractive index detectors. ^{1}H NMR spectra were measured by using a Bruker AM 500 spectrometer where with $CDCl_3$ was used as the solvent and tetramethylsilane (TMS) as an external standard. Thermal analysis was recorded by differential scanning calorimetry (DSC) using the Q20 apparatus operated between −90 and 100 °C (heating rate: 20 °C/min). Fourier transform infrared (FTIR) spectra (Bruker Tensor 27 FTIR spectrophotometer) were measured by the conventional KBr disk method. FTIR spectra measured at various temperatures were determined with the cell mounted inside the temperature-controlled compartment, which was purged with N_2 during the measurement to ensure that the samples remained dry films. Small-angle X-ray scattering (SAXS) patterns were recorded by SWAXS instrument at the BL17B3 beamline of the National Synchrotron Radiation Research Center (NSRRC), Taiwan, with a wavelength (λ) of 1.24 Å. Wide-angle X-ray scattering (WAXD) patterns were recorded using the wiggler beamline BL17A1, also at the NSRRC, with a wavelength of 1.32 Å. Transmission electron microscopy (TEM) was conducted using a JEOL-JEM-2100 microscope operated at 200 kV; ultrathin sections of phenolic/PCL-*b*-PEO-*b*-PBLG blend sample were prepared by the Leica Ultracut microtome equipped with a diamond knife; the sections were placed on a copper grid coated with a carbon supporting film; and the images were recorded after staining the samples with RuO_4.

RESULTS AND DISCUSSION

Analyses of PCL-*b*-PEO-*b*-PBLG Triblock Copolymers. We synthesized the PCL-*b*-PEO-*b*-PBLG triblock copolymers through sequential ROPs (Scheme 1). Two different degrees of polymerization (DPs) of the PBLG segments were obtained after using the amino-terminated PCL-*b*-PEO diblock copolymer ($CL_{56}EO_{40}$-NH_2) as a macroinitiator. As shown in Figure S1a, the GPC analysis of pure PCL-*b*-PEO diblock copolymer displays the monomodal trace with high symmetry and narrow polydispersity. In addition, the GPC analyses also exhibited the narrow polydispersity, with signals shifted to lower retention times indicating the formation of the PCL-*b*-PEO-*b*-PBLG triblock copolymers (Figure S1b,c and Table 1). We also determined the molecular weights based on ^{1}H NMR spectra (Figure 1). The spectrum of the diblock copolymer PCL-*b*-PEO featured signals at 3.65 ppm (peak **a**), corresponding to the ethylene units (CH_2CH_2O) of the PEO block segment, and 4.10 ppm (peak **f**) for the methylene units (OCH_2) of the PCL block segment; other signals for the methylene units of the PCL block segment are also assigned in Figure 1a. Figure 1b displays the ^{1}H NMR spectrum of the BLG monomer, where the signals at 7.36 ppm correspond to the aromatic ring

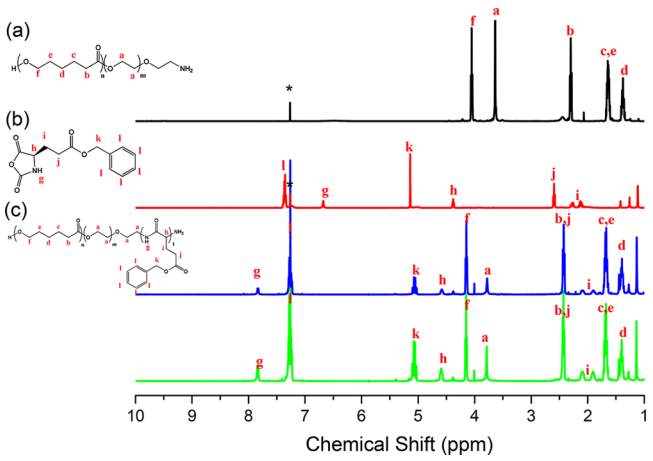

Figure 1. ^{1}H NMR spectra of (a) PCL_{56}-*b*-PEO_{40}-NH_2, (b) the BLG-NCA monomer in *d*-chloroform, (c) PCL_{56}-*b*-PEO_{40}-*b*-$PBLG_{20}$, and (c) PCL_{56}-*b*-PEO_{40}-*b*-$PBLG_{48}$ in *d*-chloroform with 15% TFA.

protons, the singlet at 6.67 ppm represents the NH unit of the ring, the signal at 5.12 ppm corresponds to the $COOCH_2C_6H_5$ unit, the signal at 4.37 ppm represents the methine unit (CH) at the α-carbon atom, and the multiplets between 2.14 and 2.60 ppm correspond to the CH_2 protons. Figures 1c and 1d display the ^{1}H NMR spectra of the PCL-*b*-PEO-*b*-PBLG triblock copolymers incorporating PBLG segments with two different DPs. A singlet for the amide proton (8.32 ppm) and a multiplet for the aromatic protons (7.26 ppm) were observed for the PBLG block segments. All other peak assignments for these PCL-*b*-PEO-*b*-PBLG triblock copolymers are summarized in Figures 1c and 1d. As a result, we also could measure the molecular weights of the PBLG block segments based on ^{1}H NMR spectra using the equation

$$M_{PBLG} = \frac{I_f \times 56}{I_k} \times M_{BLG}$$

where I_k and I_f are the intensities of the signals for $COOCH_2C_6H_5$ units of PBLG block segments and $O-CH_2$ units of PCL block segment, respectively; "56" is the DP of the PCL block segment in this study. Table 1 summarizes the molecular weights of PCL-*b*-PEO and PCL-*b*-PEO-*b*-PBLG species used in this study, based on GPC and ^{1}H NMR spectroscopy.

Figure 2 presents FTIR spectra measured at room temperature for PCL-*b*-PEO, the BLG monomer, and PCL-*b*-PEO-*b*-PBLG. The spectrum of the PCL-*b*-PEO diblock copolymer (Figure 2a) features absorption peaks at 1724 and 1734 cm^{-1}, corresponding to stretching of the crystalline and amorphous C=O units, respectively, of PCL block segment; an absorption peak at 1100 cm^{-1} corresponds to ether (C−O−C) stretching in PEO block segment. In the spectrum of the BLG monomer (Figure 2b), two typical C=O absorptions appear at 1882 and 1785 cm^{-1}, due to the C=O groups of **c** and **d**, respectively, with a peak at 1720 cm^{-1} due to the free C=O group of **e**. After NCA ROP of BLG monomer, the spectra of PCL-*b*-PEO-*b*-PBLG triblock copolymers (Figure 2c,d) featured new absorptions at 1655 cm^{-1} (**f**) and 1548 cm^{-1} (**g**) cm^{-1} due to the amide I and amide II absorption of PBLG block segments. In addition, the signal of the side chain C=O groups of PBLG block segment overlapped with the signal of the C=O units of PCL block segment near 1734 cm^{-1}, and the peak at

DOI: 10.1021/acs.macromol.8b00087
Macromolecules 2018, 51, 3017−3029

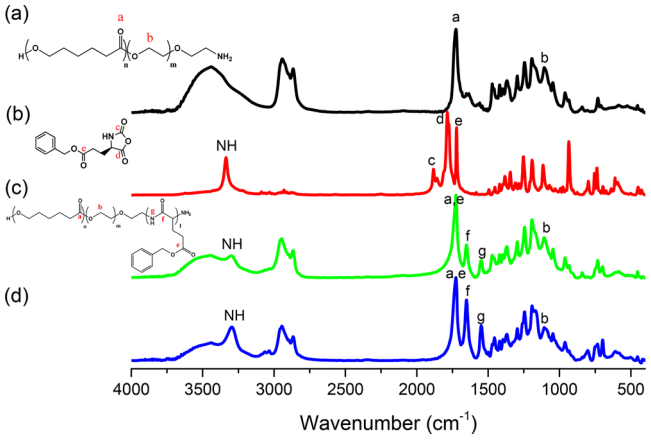

Figure 2. FTIR spectra of (a) PCL_{56}-*b*-PEO_{40}-NH_2, (b) the BLG-NCA monomer, (c) PCL_{56}-*b*-PEO_{40}-*b*-$PBLG_{20}$, and (d) PCL_{56}-*b*-PEO_{40}-*b*-$PBLG_{48}$.

1655 cm^{-1} for the α-helical conformation was observed.[54−59] As a result, the GPC, FTIR, and ^1H NMR analyses confirmed our successful syntheses of the PCL-*b*-PEO-*b*-PBLG triblock copolymer.

Self-Assembly and Secondary Structures of PCL-*b*-PEO-*b*-PBLG Triblock Copolymer. Figure 3 presents SAXS, WAXD, and TEM results, recorded at room temperature, for PCL-*b*-PEO and PCL-*b*-PEO-*b*-PBLG. SAXS analysis revealed that the pure PCL-*b*-PEO diblock copolymer had a lamellar structure with a peak ratio of 1:3, with the first maximum peak appearing at a value of q^* of 0.47 nm^{-1} (d = 13.36 nm), due to crystallization-driven microphase separation from the PCL block segment (Figure 3a). Because we observed only two strong PCL reflection peaks at values of q of 15.17 and 16.81 nm^{-1} for the (110) and (200) planes of the PCL block segment, but we did not observe the $(120)_{PEO}$ reflection peak in this diblock copolymer (Figure 3b) through WAXD analysis, we suspect that the PEO block segment could not crystallize as a result of a confinement effect for the block copolymer.[60] Figure 3c displays the TEM image of the PCL-*b*-PEO diblock copolymer, also possessing a lamellar structure (dark region: PEO block; bright region: PCL block), stained with RuO_4. In addition, the long period of the lamellar structure was approximately 15 nm, consistent with the SAXS analysis. After NCA ROP of the BLG monomer (Figure 3b,c), the PCL-*b*-PEO-*b*-PBLG triblock copolymer also exhibited a lamellar crystalline structure with peak ratios of 1:2:3:4 (Figure 3b) and 1:2 (Figure 3c) observed through SAXS analyses; two strong $(110)_{PCL}$ and $(200)_{PCL}$ reflection peaks were also observed in Figures 3e and 3f through WAXD analyses. Figures 3h and 3i display TEM images for PCL-*b*-PEO-*b*-PBLG, also possessing lamellar structures (bright region: PCL block), consistent with the SAXS analyses. Most importantly, the first maximum peaks shifted to higher values of q at a value of q^* of 0.55 nm^{-1} (d = 11.42 nm) after NCA ROP of the BLG monomer to form the triblock copolymer PCL-*b*-PEO-*b*-PBLG. The decrease in the long period of the lamellar structure of the PCL block segment was due to the increase in the cross-sectional area; thus, the PCL chains would shrink to match the increase in the interfacial area after tethering of the PBLG segment (Scheme S1a,b). The increase in the cross-sectional area after tethering the PBLG segment occurred because of the formation of long-range-ordered two-dimensional (2D) hexagonally packed cylinders with an 18/5 α-helical pitch for the PBLG block segment (Scheme S1b).

To confirm the hexagonally packed cylindrical structure, Figure 4 presents WAXD analyses of PCL-*b*-PEO-*b*-PBLG at

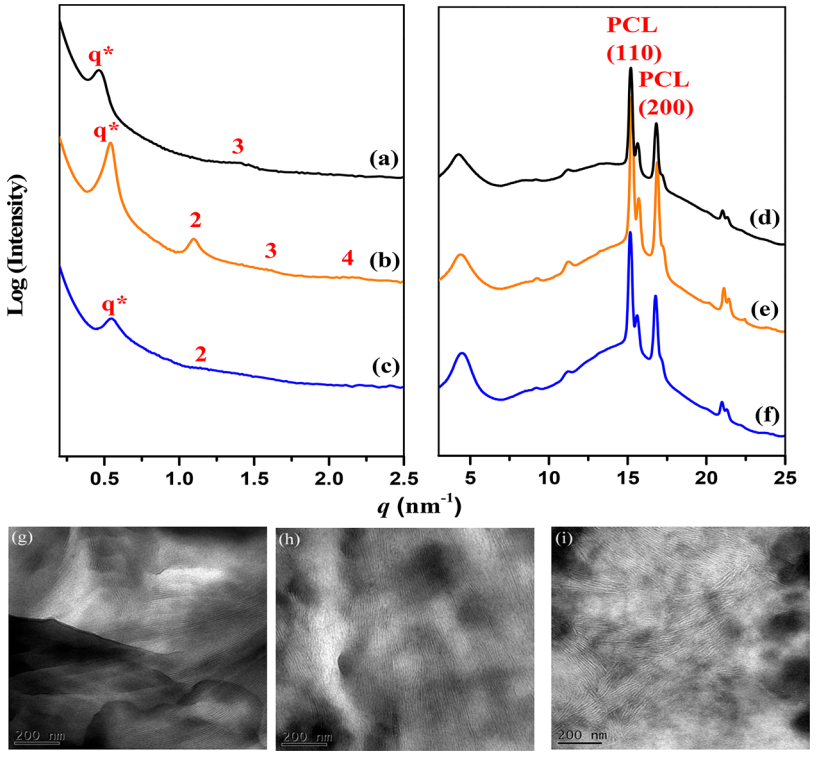

Figure 3. SAXS, WAXD, and TEM analyses of (a, d, g) PCL_{56}-*b*-PEO_{40}-NH_2, (b, e, h) PCL_{56}-*b*-PEO_{40}-*b*-$PBLG_{20}$, and (c, f, (i) PCL_{56}-*b*-PEO_{40}-*b*-$PBLG_{48}$, recorded at room temperature.

DOI: 10.1021/acs.macromol.8b00087
Macromolecules 2018, 51, 3017−3029

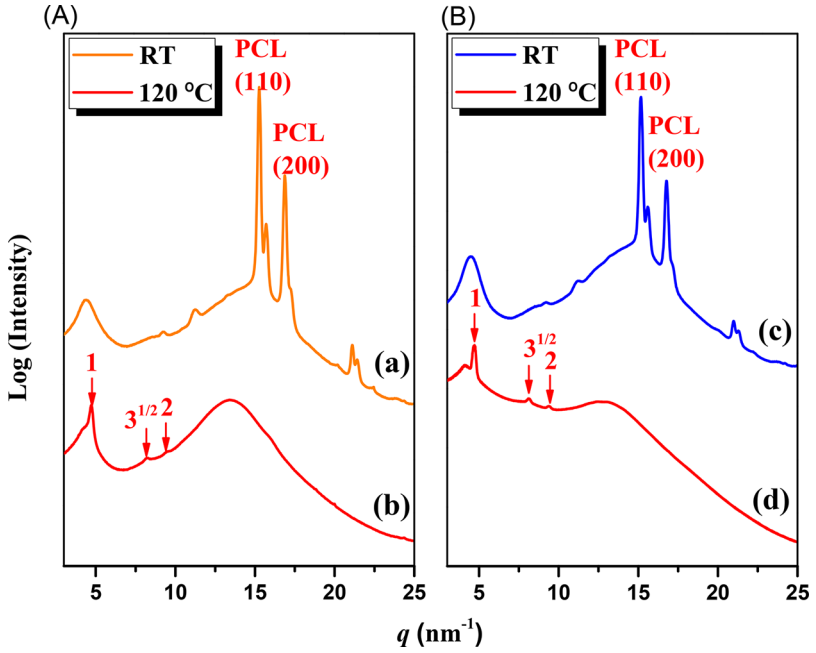

Figure 4. WAXD patterns for (a, b) PCL_{56}-*b*-PEO_{40}-*b*-$PBLG_{20}$ and (c, d) PCL_{56}-*b*-PEO_{40}-*b*-$PBLG_{48}$, recorded at (a, c) RT and (b, d) 120 °C.

room temperature and 120 °C. The crystal peak from the PCL block segment disappeared (Figure 4a,c) when the temperature (120 °C) was higher than the melting temperature of the PCL block segment (75 °C). In addition, PBLG usually displays a nematic-like liquid crystal phase transition at 100 °C during the first heating scan in DSC analyses;[50,53,55] thus, a temperature of 120 °C was higher than both the melting state of the PCL block segment and the liquid-crystalline state of the PBLG block segment. We observed an amorphous halo at higher values of q [q = 13.3 nm^{-1} (d = 0.47 nm)], arising from the molten state of the PEO and PCL segments. Strong reflection peaks appeared at values of q of 4.70, 8.14, and 9.40 nm^{-1}, with a peak ratio of $1:\sqrt{3}:\sqrt{4}$, corresponding to a hexagonally packed cylindrical structure for the PBLG block segment with a lattice parameter of approximately 1.34 nm.

From the combined SAXS and WAXD analyses, Scheme 3 suggests possible hierarchical structures formed from the PCL-*b*-PEO-*b*-PBLG triblock copolymer. First, the PEO coil, PCL crystalline, and PBLG rigid rod structures underwent microphase separation into the lamellar phase (d = 11.42 nm), where the rigid rods of the PBLG block segment were aligned parallel to the normal layer of the PCL crystalline structure (Scheme 3c,d). Second, the rigid rods of the PBLG block segment formed a hexagonally packed cylindrical structure having a diameter of approximately 1.34 nm (Scheme 3e).

Thermal Analyses of Phenolic/PCL-*b*-PEO-*b*-PBLG Blends. DSC is the well-established method for determining the miscibility behavior for polymer blend system. Figure 5 displays DSC analyses (second heating thermograms) for phenolic/PCL-*b*-PEO-*b*-PBLG blends at various compositions. In previous studies, the glass transition temperatures (T_g) of pure PEO, PCL, PBLG, and phenolic resin were determined to be −60, −60, +18, and +64 °C, respectively.[45−47] For the pure PCL-*b*-PEO-*b*-PBLG triblock copolymer, we observed two values of T_g at −60 and +18 °C, due to the PEO/PCL segments and the PBLG segment, respectively, and a melting

Scheme 3. Schematic Representation of the Hierarchical Structures of PCL-*b*-PEO-*b*-PBLG: (a, b) Chemical Structure of PCL_{56}-*b*-PEO_{40}-*b*-$PBLG_{48}$; (c) PBLG Rod, PEO Coil, and PCL Crystalline Structures in the Lamellar Structure, Where the PBLG Rods Are Aligned Parallel to the Normal Layer of the PCL Crystalline Structure; (d) PCL-*b*-PEO-*b*-PBLG Lamellar Structures; (e) PBLG Blocks Forming Hexagonally Packed Cylinders

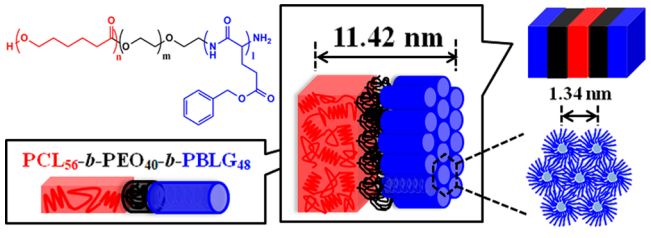

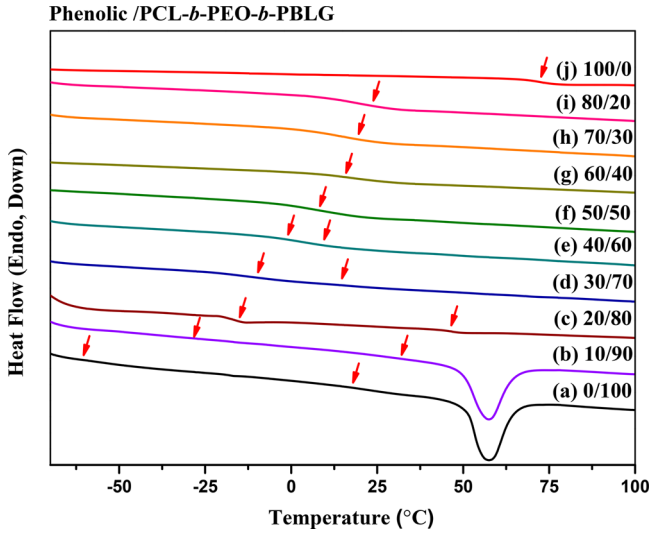

Figure 5. DSC thermograms of phenolic/PCL_{56}-*b*-PEO_{40}-*b*-$PBLG_{48}$ blends of various compositions.

DOI: 10.1021/acs.macromol.8b00087
Macromolecules 2018, 51, 3017−3029

temperature (T_m) of 54 °C corresponding to PCL block segment, as mentioned in the WAXD analyses (Figure 3). After blending with 10 wt % of phenolic, the melting peak remained near 54 °C, suggesting that the PCL block segment of crystalline structure was not destroyed. Furthermore, two values of T_g were also observed at −28 and +31 °C, also suggesting that this blend composition possessed immiscible behavior (phase separation). After blending with 20 wt % of phenolic, the melting peak (ca. 54 °C) for PCL block segment disappeared, implying that the phenolic OH groups interacted with the C═O groups of the PCL block, thereby destroying the crystalline structure of PCL block segment. In addition, two clear T_g values appeared at −15 and +45 °C, implying that this blend composition also exhibited immiscible behavior. Further increasing the content of phenolic to 30 and 40 wt %, two values of T_g still remained but shifted close together. More interestingly, a single T_g value appeared at phenolic concentration greater than 50 wt %, implying that the phenolic OH groups interacted with all of the block segments through hydrogen bonding, thereby inducing totally miscible behavior at higher phenolic contents. Table 2 summarizes the experimental

Table 2. Thermal Analysis Data for Phenolic/PCL-*b*-PEO-*b*-PBLG Blends

phenolic/PCL-*b*-PEO-*b*-PBLG	experimental T_g (°C)		theoretical T_g (°C)
100/0	64		
80/20	23		46
70/30	19		37
60/40	15		28
50/50	8		19
40/60	−1	10	
30/70	−10	15	
20/80	−15	46	
10/90	−28	31	
0/100	−60	18	

T_g values of the phenolic/PCL-*b*-PEO-*b*-PBLG blends in this study. The values of T_g for the miscible compositions were lower than those calculated from the linear rule, implying that the average hydrogen bonding strength in the miscible phenolic/PCL-*b*-PEO-*b*-PBLG phase was weaker than the self-association (OH---OH) hydrogen bonding of phenolic resin at relatively high phenolic contents. Here, we conclude that immiscible behavior or phase separation occurred at phenolic concentration less than 40 wt %, but miscible behavior occurred when the phenolic concentration was greater than 50 wt % since the phenolic OH groups interacted with all the block segments through hydrogen bonding, as confirmed through FTIR spectroscopic analyses (see next section).

FTIR Spectral Analyses of Phenolic/PCL-*b*-PEO-*b*-PBLG Blends. Since the phenolic OH groups could interact with all of the PCL, PEO, and PBLG block segments through hydrogen bonding when the phenolic content was greater than 50 wt % and, thereby, induce miscible behavior, we used FTIR spectroscopy to examine whether the phenolic resin could act as a common solvent in these phenolic/PCL-*b*-PEO-*b*-PBLG blends. Figure 6 displays the FTIR spectra [(A) OH, (B) C═O, (C) C−O−C regions] of various phenolic/PCL-*b*-PEO-*b*-PBLG blends at room temperature. Pure phenolic displayed two unresolved absorption in the OH region (Figure 6A-j): a broad band for the self-association hydrogen-bonded OH groups at 3380 cm^{-1}, but a narrow band for the free OH groups at 3525 cm^{-1}. For pure PCL-*b*-PEO-*b*-PBLG (Figure 6A-a), we observed a sharp absorption at 3300 cm^{-1} due to the NH stretching in the peptide bonds of the PBLG block segment. Clearly, the intensity of free OH unit decreased upon increasing the concentration of PCL-*b*-PEO-*b*-PBLG triblock copolymer. Table 3 summarizes the thermodynamic properties of phenolic/PCL-*b*-PEO-*b*-PBLG blends tested in this study; the measured interassociation values for phenolic/PEO (K_A = 264.8), phenolic/PCL (K_C = 116.8), and phenolic/PLBG (K_D = 9.0) suggested that the strength of hydrogen bonding in the binary blends followed the order phenolic/PEO > phenolic/PCL > phenolic/PBLG (Scheme 2). Therefore, the broad OH absorption shifted to lower wavenumber at 3200 cm^{-1} at a relatively lower phenolic content of 10 wt %, indicating that the phenolic OH groups interact only with the C−O−C units in the PEO block segment. In addition, the broad OH absorption shifted to higher wavenumber at 3465 cm^{-1} upon increasing the phenolic concentration to greater than 30 wt %, reflecting a new distribution of hydrogen bonding from OH---ether interactions of phenolic/PEO to OH---C═O interactions of phenolic and the PCL or PBLG block segments. Nevertheless, we also observed that the signal for NH stretching did not change upon increasing phenolic concentration, indicative of no hydrogen bonding between the NH units of PBLG and the OH units of phenolic resin.[51] Therefore, intermolecular hydrogen bonding existed only between phenolic OH groups and the PEO ether units, the PCL and PBLG C═O units.

Figure 6B displays the C═O units in the FTIR spectra of phenolic/PCL-*b*-PEO-*b*-PBLG blends of various compositions. We observed an absorption at 1655 and 1544 cm^{-1} (Figure S2) for the α-helical conformation of the PBLG block segment and peaks at 1724 and 1734 cm^{-1} corresponding to crystalline and amorphous C═O stretching of PCL block segment. The signal for the side chain C═O groups of the PBLG block segment, however, overlapped with the signal for the C═O groups of the PCL block segment at 1734 cm^{-1} for pure PCL-*b*-PEO-*b*-PBLG triblock copolymer (Figure 6B-a). Clearly, the signal of the α-helical conformation at 1655 and 1544 cm^{-1} (Figure S2) remained upon increasing the phenolic content, consistent with previous studies in which we found that strong hydrogen bonding could stabilize the α-helical conformations of PBLG segments.[51,61,62] When blended with 10 wt % phenolic resin, the absorption at 1724 cm^{-1}, representing the crystalline structure, remained, implying that the crystalline structure from the PCL segment was not destroyed, again consistent with the DSC analysis at this composition. Because the phenolic/PEO hydrogen bonding should have dominated at relatively low phenolic contents, we expected the phenolic OH groups to interact only with the C−O−C units in the PEO segment at 10 wt % phenolic resin. In the spectra displaying the C−O−C region (Figure 6C), the band at 1108 cm^{-1} (representing the C−O−C units in the PEO block segment) shifted to 1100 cm^{-1} due to the hydrogen bonding of the C−O−C units, as the phenolic concentration was greater than 20 wt %. This result indicates that the phenolic OH groups interacted with the C═O groups of the PCL block segment, and even with the C═O groups of the PBLG block segment, at relatively high phenolic contents. As a result, the signal for the crystalline conformation at 1724 cm^{-1} disappeared, and a signal appeared at 1734 cm^{-1} for the amorphous conformation or free C═O groups of the PCL or PBLG block segment, consistent with the DSC analysis where the melting peak disappeared at a phenolic resin content

DOI: 10.1021/acs.macromol.8b00087
Macromolecules 2018, 51, 3017−3029

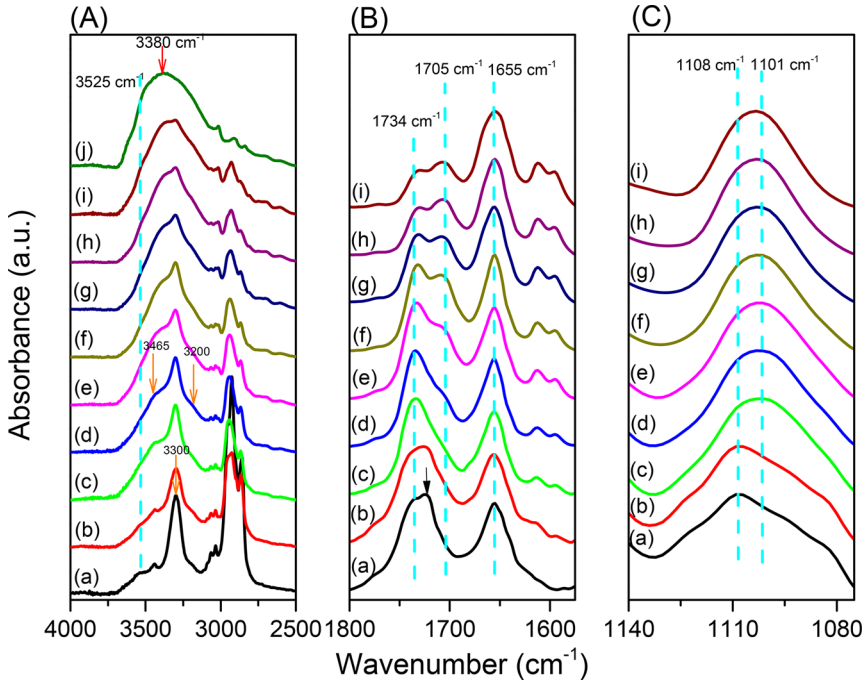

Figure 6. FTIR spectra of phenolic/$CL_{56}EO_{40}BLG_{48}$ blends, recorded at room temperature: (A) OH, (B) C═O, and (C) ether regions, at compositions of (a) 0/100, (b) 10/90, (c) 20/80, (d) 30/70, (e) 40/60, (f) 50/50, (g) 60/40, (h) 70/30, (i) 80/20, and (j) 100/0.

Table 3. Thermodynamic Parameters and Self- and Interassociation Equilibrium Constants for Phenolic/PCL-*b*-PEO-*b*-PBLG Blends at 25 °C[a]

				equilibrium constants				
polymer	molar volume (mL/mol)	molecular weight (g/mol)	solubility parameter ((cal/mL)$^{1/2}$)	K_2	K_B	K_A	K_C	K_D
phenolic	84.0	105	12.0	23.3	52.3			
PEO	38.1	44.1	9.40			264.8		
PCL	102.1	114.1	9.21				116.8	
PBLG	165.9	219.0	11.2					9.0

[a]Self-association equilibrium constant: K_2 (dimer) and K_B (multimer); interassociation equilibrium constants: K_A, K_C, and K_D.

of 20 wt %. Furthermore, we observed a new absorption at 1705 cm^{-1}, corresponding to hydrogen-bonded C═O units of the PCL or PBLG block, when the phenolic concentration was greater than 20 wt %, implying that the phenolic OH groups had begun to interact with the PCL and PBLG C═O groups. Notably, the signal for the hydrogen-bonded C═O groups of the PBLG segment shifted only to 1710 cm^{-1} with the increase of phenolic concentration[47] because of their relatively weak hydrogen bonding (K_A = 9.0) compared with that of phenolic/PCL binary blend system (K_A = 116.8). For convenience, we considered the signal at 1705 cm^{-1} as a combination of the signals of the hydrogen-bonded C═O groups of both PCL and PBLG because the presence of many absorption peaks made it difficult to determine the quantitative fraction of hydrogen-bonded C═O groups. Therefore, we simplified the C═O region in the FTIR spectra of the phenolic/PCL-*b*-PEO-*b*-PBLG blends to feature only two main bands representing the hydrogen-bonded and free C═O groups of PCL and PBLG at 1705 and 1734 cm^{-1}, respectively. This system was readily decomposed into Gaussian distributions; Table 4 lists the results obtained through curve fitting. The fraction of hydrogen-bonded C═O groups in this blend system could be determined using the appropriate absorptivity ratio [a = 1.5 (a_{HB}/a_F)] for interassociation hydrogen-bonded OH---O═C

Table 4. FTIR Spectroscopic Data for Phenolic/PCL-*b*-PEO-*b*-PBLG Blends

	FTIR signals				
	free C═O		hydrogen-bonded C═O		
phenolic/PCL-*b*-PEO-*b*-PBLG	ν (cm^{-1})	A_f (%)	ν (cm^{-1})	A_f (%)	$f_b^{C=O}$
0/100	1734	100.0			0
20/80	1734	82.86	1710	17.14	0.121
30/70	1734	78.14	1710	21.86	0.157
40/60	1734	67.60	1709	32.40	0.242
50/50	1734	56.06	1709	43.94	0.343
60/40	1734	48.97	1709	51.03	0.409
70/30	1733	43.81	1708	56.19	0.460
80/20	1733	36.15	1708	63.85	0.540

units,[48] suggesting that the fraction of hydrogen-bonded C═O units increased with the increase of the phenolic concentration.

To better understand the hydrogen bonding interactions in phenolic/PCL-*b*-PEO-*b*-PBLG blends, Figure S3 summarizes the C═O region in the FTIR spectra of (A) phenolic/PCL, (B) phenolic/PCL-*b*-PEO, (C) phenolic/PCL-*b*-PEO-*b*-PBLG, and (D) phenolic/PBLG blend systems. The fraction of hydrogen-bonded C═O units was increased with the increase

DOI: 10.1021/acs.macromol.8b00087
Macromolecules 2018, 51, 3017−3029

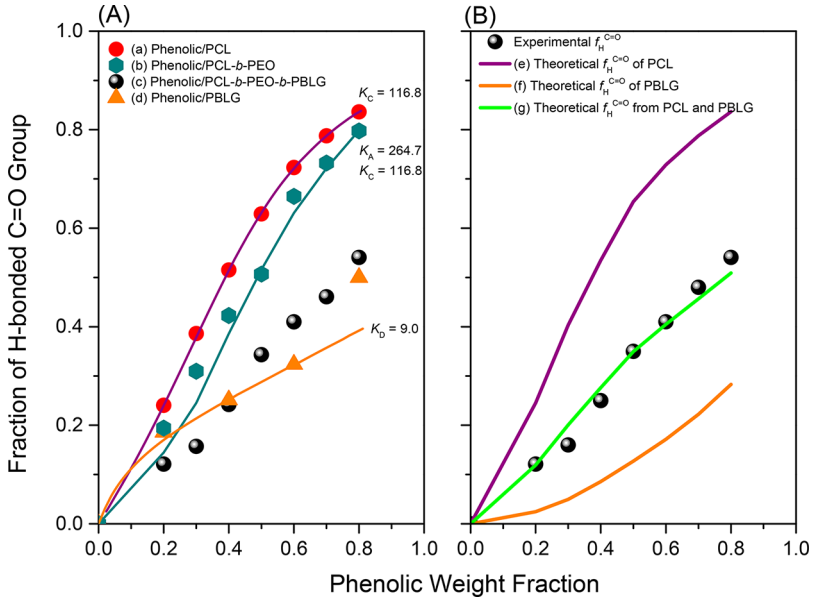

Figure 7. (A) Theoretical and experimental fractions of hydrogen-bonded C═O groups for (a) phenolic/PCL, (b) phenolic/PCL-*b*-PEO, (c) phenolic/PCL-*b*-PEO-*b*-PBLG, and (d) phenolic/PBLG blends. (B) Theoretical fractions of hydrogen-bonded C═O groups for (e) PCL, (f) PBLG, and (g) PCL and PBLG block segments and experimental results in this phenolic/PCL-*b*-PEO-*b*-PBLG blend system.

of phenolic concentration for all four blend systems; Figure 7A summarizes the results. In this study, we have at least four competing functional units that affected the fraction of hydrogen-bonded C═O groups. Assigning B, A, C, and D to phenolic, PEO, PCL, and PBLG, respectively, we obtain the following equilibrium constants K_2, K_B, K_A, K_C, and K_D:

$$B_1 + B_1 \overset{K_2}{\longleftrightarrow} B_2 \tag{1}$$

$$B_h + B_1 \overset{K_B}{\longleftrightarrow} B_{h+1} \quad (h \geq 2) \tag{2}$$

$$B_h + A_1 \overset{K_A}{\longleftrightarrow} B_hA \tag{3}$$

$$B_h + C_1 \overset{K_c}{\longleftrightarrow} B_hC \tag{4}$$

$$B_h + D_1 \overset{K_c}{\longleftrightarrow} B_hD \tag{5}$$

These five equilibrium constants can be described in terms of volume fractions:

$$\Phi_B = \Phi_{B1}\Gamma_2\left[1 + \frac{K_A\Phi_{A1}}{r_A} + \frac{K_C\Phi_{C1}}{r_C} + \frac{K_D\Phi_{D1}}{r_D}\right] \tag{6}$$

$$\Phi_A = \Phi_{A1}[1 + K_A\Phi_{B1}\Gamma_1] \tag{7}$$

$$\Phi_C = \Phi_{C1}[1 + K_C\Phi_{B1}\Gamma_1] \tag{8}$$

$$\Phi_D = \Phi_{D1}[1 + K_D\Phi_{B1}\Gamma_1] \tag{9}$$

where

$$\Gamma_1 = \left(1 - \frac{K_2}{K_B}\right) + \frac{K_2}{K_B}\left(\frac{1}{(1 - K_B\Phi_{B1})}\right) \tag{10}$$

$$\Gamma_2 = \left(1 - \frac{K_2}{K_B}\right) + \frac{K_2}{K_B}\left(\frac{1}{(1 - K_B\Phi_{B1})^2}\right) \tag{11}$$

Here, Φ_A, Φ_B, Φ_C, and Φ_D represent the volume fraction of each block segments in the blend system; Φ_{A1}, Φ_{B1}, Φ_{C1}, and Φ_{D1} represent the volume fraction of each free unit in blend system; and r_A (V_A/V_B), r_C (V_C/V_B), and r_D (V_D/V_B) are the molar volume ratios of each block segment in the presence of phenolic resin. Table 3 displays the self-association equilibrium constants for phenolic (K_2 = 23.3 and K_B = 52.3) and the interassociation equilibrium constants for phenolic/PEO, phenolic/PCL, and phenolic/PBLG blends (264.8, 116.8, and 9.0, respectively).[49−51] In Figure 7A, the experimental results reveal that the fraction of hydrogen-bonded C═O groups for PCL or PBLG increased upon increasing the phenolic content and could be predicted by the PCAM, in the phenolic/PCL, phenolic/PCL-*b*-PEO, and phenolic/PBLG blend systems. The fraction of hydrogen-bonded C═O groups for PCL reached its highest value at the same phenolic content as shown in Figure 7A-a; this fraction in the phenolic/PCL-*b*-PEO blend system (Figure 7A-b) decreased compared with that in the phenolic/PCL blend because the phenolic OH groups preferred to interact with the ether units in the PEO block (i.e., largest value of K_A was that for the phenolic/PEO blend). Furthermore, the fraction of hydrogen-bonded C═O units for PBLG was lower (Figure 7A-d) than those for the phenolic/PCL and phenolic/PCL-*b*-PEO blend systems at the same phenolic concentration due to the phenolic/PBLG blend having the lowest value of K_A. On the basis of eqs 6−11, we measured the theoretical fractions of hydrogen-bonded C═O groups for the PCL and PBLG block segments (Figures 7B-e and 7B-g); unfortunately, the signal for the side-chain C═O groups of the PBLG block segment overlapped with that for the C═O groups of the PCL block segment in the FTIR spectra of this triblock copolymer. Therefore, we considered the theoretical fraction of hydrogen-bonded C═O groups in the phenolic/PCL-*b*-PEO-*b*-PBLG blend to be equal to (Φ_{PCL} × curve Figure 7B-e + Φ_{PBLG} × curve Figure 7B-g); Figure 7B-f reveals that we could predict the experimental results quite well. To the best of our knowledge, this study is the first to accurately predict the

DOI: 10.1021/acs.macromol.8b00087
Macromolecules 2018, 51, 3017−3029

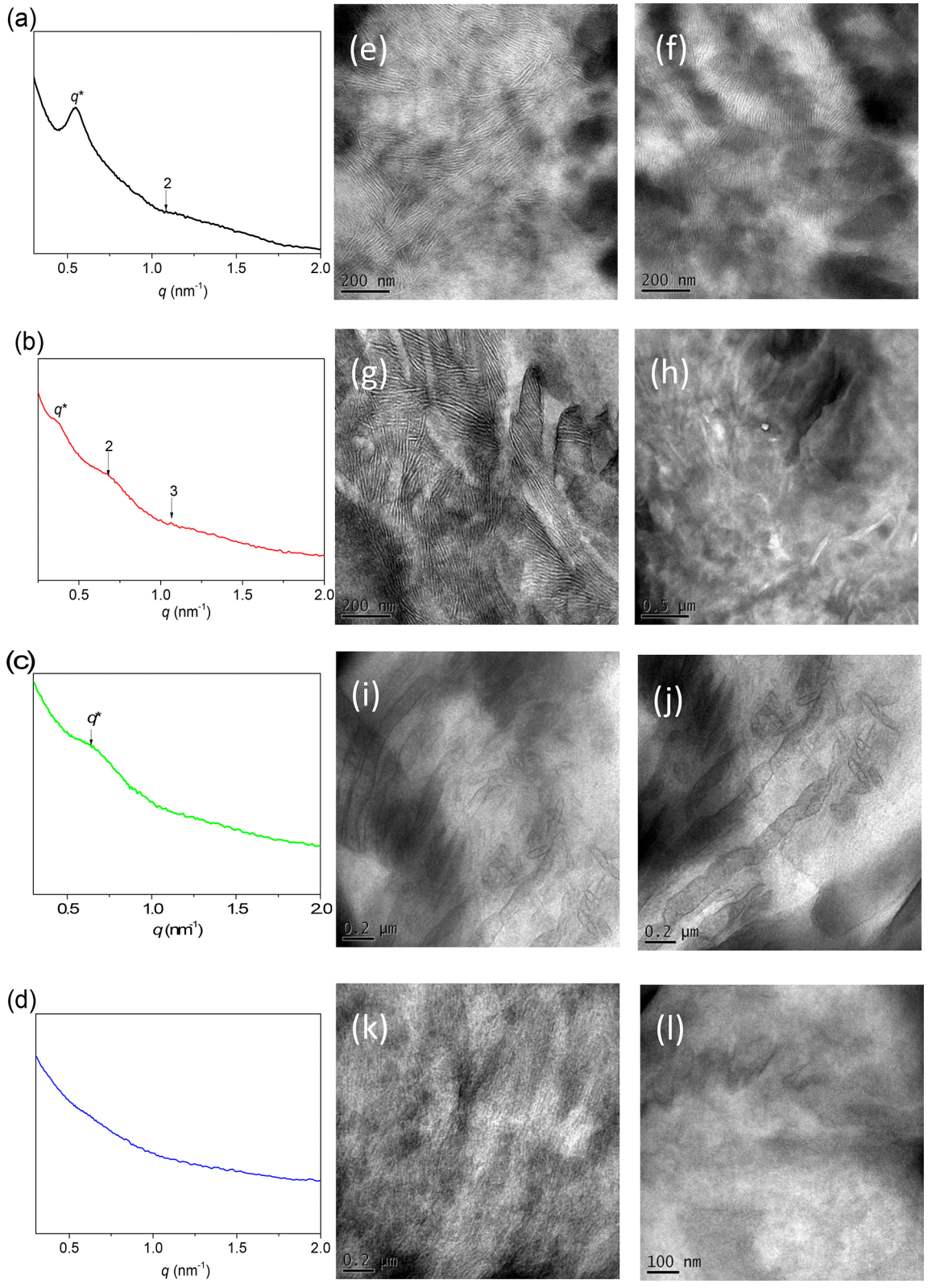

Figure 8. SAXS patterns and TEM images of phenolic/PCL-*b*-PEO-*b*-PBLG blends: (a, e, f) 0/100, (b, g, h) 10/90, (c, i, j) 20/80, and (d, k, l) 40/60.

hydrogen bonding behavior of a system containing four competing functional units.

Self-Assembly and Secondary Structures of Phenolic/PCL-*b*-PEO-*b*-PBLG Blends. Figure 8 presents SAXS and TEM data, recorded at room temperature, for phenolic/PCL-*b*-PEO-*b*-PBLG blends. The SAXS analysis of the pure PCL-*b*-PEO-*b*-PBLG triblock copolymer reveals a lamellar crystalline structure with a peak ratio of 1:2 (Figure 8a), as confirmed through TEM (Figures 8e and 8f). When blended with 10 wt % phenolic resin, SAXS also revealed a lamellar crystalline

DOI: 10.1021/acs.macromol.8b00087
Macromolecules 2018, 51, 3017−3029

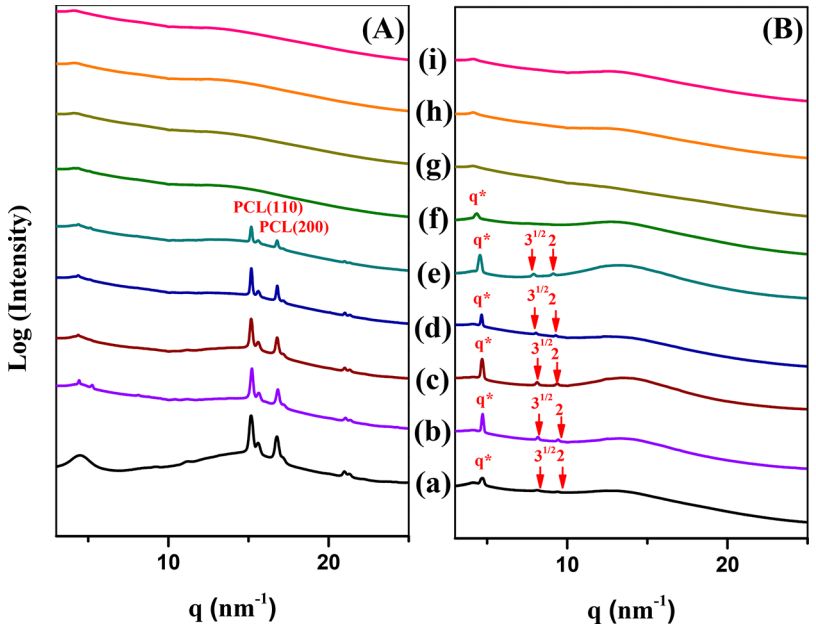

Figure 9. WAXD patterns of phenolic/PCL-*b*-PEO-*b*-PBLG blends recorded at (A) RT and (B) 120 °C at compositions of (a) 0/100, (b) 10/90, (c) 20/80, (d) 30/70, (e) 40/60, (f) 50/50, (g) 60/40, (h) 70/30, and (i) 80/20.

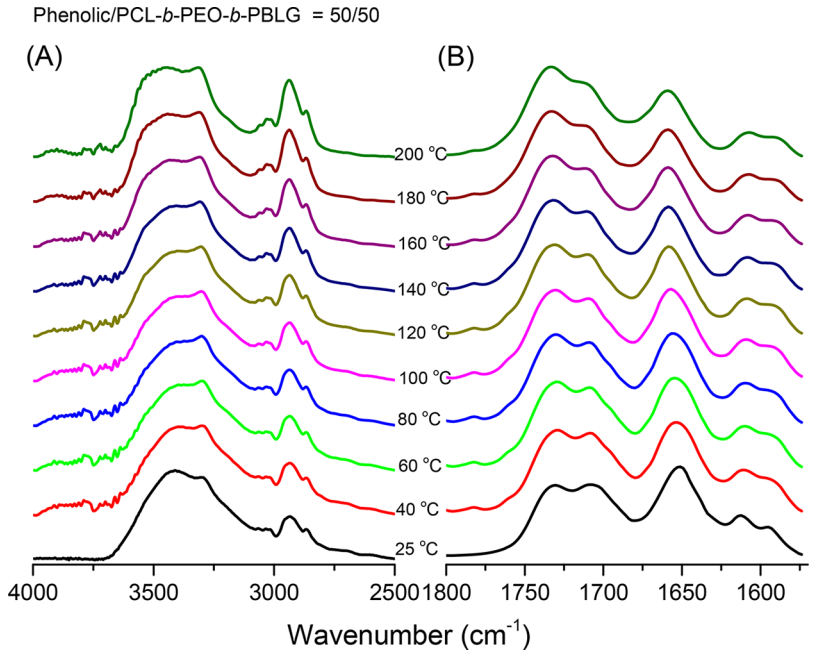

Figure 10. FTIR spectra of the phenolic/PCL-*b*-PEO-*b*-PBLG = 50/50 blend, recorded at various temperatures: (A) OH and (B) C═O regions.

structure with a peak ratio of 1:2:3 (Figure 8b), again confirmed by TEM (Figures 8g and 8h). In addition, we observed that the first maximum peak was shifted from a value of q^* of 0.55 nm^{-1} (d = 11.42 nm) to a lower value of q at a value of q^* of 0.36 nm^{-1} (d = 17.4 nm), suggesting an increase in the d-spacing upon blending with phenolic resin. When the phenolic content was 20 wt %, only one broad peak appeared at a value of q^* of 0.64 nm^{-1}, suggesting the short-range order of a micelle structure, as confirmed through TEM analyses (Figures 8i and 8j) and consistent with the DSC and FTIR spectroscopic analysis [recall that the melting peak (T_m = 54 °C) and the signal representing the crystalline conformation at 1724 cm^{-1} both disappeared at 20 wt % phenolic resin]. A further increase in the phenolic content to 40 wt % resulted in the disordered structure being observed through SAXS (Figure 8d) and TEM (Figures 8k and 8l). At this composition, the OH groups of phenolic would interact with all the block segments in PCL-*b*-PEO-*b*-PBLG, inducing a miscible disordered structure at higher phenolic contents, as revealed in the FTIR spectroscopic and DSC analyses. Unfortunately, we did not observe hierarchical nanostructures arising from microphase separation from the PCL and PBLG block segments, possibly because the slight differences in the values of K_A of the PEO, PCL, and PBLG block segments could not induce highly ordered self-assembled structures in this competitive hydrogen bonding blend system.[15]

DOI: 10.1021/acs.macromol.8b00087
Macromolecules 2018, 51, 3017−3029

Figure 9 presents WAXD analyses of phenolic/PCL-*b*-PEO-*b*-PBLG blends measured at room temperature and 120 °C. The crystal peaks of $(110)_{PCL}$ and $(200)_{PCL}$ from the PCL block segment disappeared at 50 wt % phenolic resin (Figure 10A). Nonetheless, this phenomenon is different from the behavior in the DSC thermal analyses (Figure 5), where the crystalline peak disappeared at 20 wt % phenolic resin, possibly because of the different methods of sample preparation. The polymer crystallinity measured using DSC analysis is strongly dependent on the thermal history because recrystallization would occur during the heating and cooling scans. In contrast, the polymer crystallinity determined through WAXD analysis is an in situ characteristic, with no thermal history. Furthermore, characterization of polymer crystallinity based on the WAXD analysis may be more sensitive than that through DSC analysis. Similar to Figure 4, the crystal peaks from the PCL block segment disappeared (Figure 9B) when the temperature (120 °C) was higher than both the melting state of the PCL block segment and the liquid-crystalline state of the PBLG block segment. We observed strong reflection peaks with the peak ratio of $1:\sqrt{3}:\sqrt{4}$, also corresponding to the hexagonally packed cylindrical structure, as the phenolic concentration was less than 50 wt %. This result indicates that phenolic OH groups had begun to interact with the C═O groups of the PBLG and then induced the miscible ordered structure. In addition, the first maximum peak shifted slightly from a value of q^* of 4.70 nm^{-1} (d = 1.334 nm) to a lower value of q at a value of q^* of 4.68 nm^{-1} (d = 1.342 nm), suggestion the d-spacing increase of the lattice parameter upon blending with the phenolic. Because the phenolic OH groups would prefer to interact with the PEO and PCL block segments at lower phenolic concentration, as shown in Figure 8B, the increase or swelling of the d-spacing of the hexagonally packed cylinders was due to the increase in the cross-sectional area between the PEO (or PCL) block segment and the PBLG block segment (Scheme S2).

Figure 10 displays FTIR spectra of the phenolic/PCL-*b*-PEO-*b*-PBLG = 50/50 blend recorded at various temperatures. In Figure 10A, the broad band for OH stretching shifted from 3415 to 3525 cm^{-1} upon increasing the temperature, suggesting that the interassociation hydrogen bonds were disrupted to form free OH groups. In Figure 10B, the fractions of hydrogen-bonded C═O groups of PCL and PBLG both decreased upon increasing the temperature, from 0.343 at room temperature to 0.278 at 200 °C, consistent with Figure 10A. In addition, the absorption peak at 1655 cm^{-1} for the α-helical conformation was not destroyed, indicating a stabile α-helical conformation in this blend system that was not affected by the temperature. We conclude that competing hydrogen bonding interactions occurred and were influenced by the phenolic content, with the composition of the block segment and the temperature also changing the miscibility, self-assembly, and secondary structures formed in this phenolic/PCL-*b*-PEO-*b*-PBLG blend system

CONCLUSIONS

We have synthesized new PCL-*b*-PEO-*b*-PBLG triblock copolymers through sequential ROPs. We have used DSC, FTIR, SAXS, WAXD, and TEM analyses to determine the miscibility and secondary and self-assembled structures formed from these triblock copolymers in the presence and absence of a phenolic resin. DSC and FTIR spectroscopy suggested that the phenolic OH groups preferred to interact with the PEO block segment at lower phenolic content but interacted with all of the PEO, PCL, and PBLG blocks at higher phenolic content. In addition, on the basis of the PCAM, we could accurately predict the fractions of hydrogen bonding interactions of the four competing functional units in this phenolic/PCL-*b*-PEO-*b*-PBLG blend system. SAXS, WAXD, and TEM analyses confirmed that these competing hydrogen bonding interactions affected the miscibility behavior and self-assembled structures formed in the presence of phenolic at various contents.

ASSOCIATED CONTENT

Supporting Information

The Supporting Information is available free of charge on the ACS Publications website at DOI: 10.1021/acs.macromol.8b00087.

Schemes S1 and S2; Figures S1−S3 (PDF)

AUTHOR INFORMATION

Corresponding Author

*E-mail kuosw@faculty.nsysu.edu.tw (S.-W.K.).

ORCID

Tao Chen: 0000-0001-9704-9545

Shiao-Wei Kuo: 0000-0002-4306-7171

Notes

The authors declare no competing financial interest.

ACKNOWLEDGMENTS

This study was supported financially by the Ministry of Science and Technology, Taiwan, under Contracts MOST 106-2221-E-110-067-MY3 and 105-2221-E-110-092-MY3. This work also supported by the National Natural Science Foundation of China (51773214).

REFERENCES

(1) Jiang, M.; Xie, H. Miscibility and morphology in block copolymer/homopolymer blends. *Prog. Polym. Sci.* **1991**, *16*, 977−1026.

(2) Zhao, J. Q.; Pearce, E. M.; Kwei, T. K. Binary and ternary blends of polystyrene-*block*-poly(*p*-hydroxystyrene). *Macromolecules* **1997**, *30*, 7119−7126.

(3) Dobrosielska, K.; Wakao, S.; Takano, A.; Matsushita, Y. Nanophase-separated structures of AB block copolymer/C homopolymer blends with complementary hydrogen-bonding interactions. *Macromolecules* **2008**, *41*, 7695−7698.

(4) Dobrosielska, K.; Wakao, S.; Suzuki, J.; Noda, K.; Takano, A.; Matsushita, Y. Effect of homopolymer molecular weight on nanophase-separated structures of AB block copolymer/C homopolymer blends with hydrogen-bonding interactions. *Macromolecules* **2009**, *42*, 7098−7102.

(5) Chen, S. C.; Kuo, S. W.; Jeng, U. S.; Su, C. J.; Chang, F. C. On modulating the phase behavior of block copolymer/homopolymer blends via hydrogen bonding. *Macromolecules* **2010**, *43*, 1083−1092.

(6) Tsai, S. C.; Lin, Y. C.; Lin, E. L.; Chiang, Y. W.; Kuo, S. W. Hydrogen bonding strength effect on self-assembly supramolecular structures of diblock copolymer/homopolymer blends. *Polym. Chem.* **2016**, *7*, 2395−2409.

(7) Dehghan, A.; Shi, A. C. Modeling hydrogen bonding in diblock copolymer/homopolymer blends. *Macromolecules* **2013**, *46*, 5796−5805.

(8) Hameed, N.; Guo, Q. Nanostructure and hydrogen bonding in interpolyelectrolyte complexes of poly(ε-caprolactone)-*block*-poly(2-vinyl pyridine) and poly(acrylic acid). *Polymer* **2008**, *49*, 5268−5275.

(9) Hameed, N.; Liu, J.; Guo, Q. Self-assembled complexes of poly(4-vinylphenol) and poly(ε-caprolactone)-*block*-poly (2-vinylpyridine) via competitive hydrogen bonding. *Macromolecules* **2008**, *41*, 7596−7605.

DOI: 10.1021/acs.macromol.8b00087
Macromolecules 2018, 51, 3017−3029

(10) Hameed, N.; Guo, Q. Selective hydrogen bonding and hierarchical nanostructures in poly(hydroxyether of bisphenol A)/poly(ε-caprolactone)-*block*-poly(2-vinyl pyridine) blends. *Polymer* **2008**, *49*, 922−933.
(11) Chen, W. C.; Kuo, S. W.; Lu, C. H.; Jeng, U. S.; Chang, F. C. Self-assembly structures through competitive interactions of crystalline−amorphous diblock copolymer/homopolymer blends: Poly(ε-caprolactone-b-4-vinyl pyridine)/poly(vinyl phenol). *Macromolecules* **2009**, *42*, 3580−3590.
(12) Salim, N. V.; Hanley, T.; Guo, Q. Microphase separation through competitive hydrogen bonding in double crystalline diblock copolymer/homopolymer blends. *Macromolecules* **2010**, *43*, 7695−7704.
(13) Li, J. G.; Lin, Y. D.; Kuo, S. W. From microphase separation to self-organized mesoporous phenolic resin through competitive hydrogen bonding with double-crystalline diblock copolymers of poly(ethylene oxide-b-ε-caprolactone). *Macromolecules* **2011**, *44*, 9295−9309.
(14) Salim, N. V.; Hameed, N.; Guo, Q. Competitive hydrogen bonding and self-assembly in poly(2-vinyl pyridine)-*block*-poly(methyl methacrylate)/poly(hydroxyether of bisphenol A) blends. *J. Polym. Sci., Part B: Polym. Phys.* **2009**, *47*, 1894−1905.
(15) Hameed, N.; Salim, N. V.; Guo, Q. Microphase separation through competitive hydrogen bonding in self-assembled diblock copolymer/homopolymer complexes. *J. Chem. Phys.* **2009**, *131*, 214905.
(16) Lee, H. F.; Kuo, S. W.; Huang, C. F.; Lu, J. S.; Chan, S. C.; Wang, C. F.; Chang, F. C. Hydrogen-bonding interactions mediate the phase behavior of an AB/C block copolymer/homopolymer blend comprising poly (methyl methacrylate-b-vinylpyrrolidone) and poly (vinylphenol). *Macromolecules* **2006**, *39*, 5458−5465.
(17) Chen, W. C.; Kuo, S. W.; Jeng, U. S.; Chang, F. C. Self-assembly through competitive interactions of miscible diblock copolymer/homopolymer blends: Poly (vinylphenol-b-methyl methacrylate)/poly (vinylpyrrolidone) blend. *Macromolecules* **2008**, *41*, 1401−1410.
(18) Zhou, J.; Shi, A. C. Microphase separation induced by differential interactions in diblock copolymer/homopolymer blends. *J. Chem. Phys.* **2009**, *130*, 234904.
(19) Lin, I.; Kuo, S. W.; Chang, F. C. Self-assembly structures through competitive interactions of miscible crystalline−amorphous diblock copolymer/homopolymer blends. *Polymer* **2009**, *50*, 5276−5287.
(20) Han, S. H.; Pryamitsyn, V.; Bae, D.; Kwak, J.; Ganesan, V.; Kim, J. K. Highly asymmetric lamellar nanopatterns via block copolymer blends capable of hydrogen bonding. *ACS Nano* **2012**, *6*, 7966−7972.
(21) Kwak, J.; Han, S. H.; Moon, H. C.; Kim, J. K.; Koo, J.; Lee, J. S.; Pryamitsyn, V.; Ganesan, V. Phase behavior of binary blend consisting of asymmetric polystyrene-*block*-poly(2-vinylpyridine) copolymer and asymmetric deuterated polystyrene-*block*-poly(4-hydroxystyrene) copolymer. *Macromolecules* **2015**, *48*, 1262−1266.
(22) Pryamitsyn, V.; Han, S. H.; Kim, J. K.; Ganesan, V. Curvature modification of block copolymer microdomains using blends of bock copolymers with hydrogen bonding interactions. *Macromolecules* **2012**, *45*, 8729−8742.
(23) Han, S. H.; Kim, J. K.; et al. Phase behavior of binary blends of block copolymers having hydrogen bonding. *Macromolecules* **2011**, *44*, 4970−4976.
(24) Kwak, J.; Han, S. H.; Moon, H. C.; Kim, J. K.; et al. Effect of the degree of hydrogen bonding on asymmetric lamellar microdomains in binary block copolymer blends. *Macromolecules* **2015**, *48*, 6347−6352.
(25) Asari, T.; Matsuo, S.; Takano, A.; Matsushita, Y. Three-phase hierarchical structures from AB/CD diblock copolymer blends with complemental hydrogen bonding interaction. *Macromolecules* **2005**, *38*, 8811−8815.
(26) Jiang, S.; Gopfert, A.; Abetz, V. Novel morphologies of block copolymer blends via hydrogen bonding. *Macromolecules* **2003**, *36*, 6171−6177.
(27) Kuo, S. W. Hydrogen bond-mediated self-assembly and supramolecular structures of diblock copolymer mixtures. *Polym. Int.* **2009**, *58*, 455−464.
(28) Chen, W. C.; Kuo, S. W.; Chang, F. C. Self-assembly of an A−B diblock copolymer blended with a C homopolymer and a C−D diblock copolymer through hydrogen bonding interaction. *Polymer* **2010**, *51*, 4176−4184.
(29) Asari, T.; Arai, S.; Takano, A.; Matsushita, Y. Archimedean tiling structures from ABA/CD block copolymer blends having intermolecular association with hydrogen bonding. *Macromolecules* **2006**, *39*, 2232−2237.
(30) Matsushita, Y. Creation of hierarchically ordered nanophase structures in block polymers having various competing interactions. *Macromolecules* **2007**, *40*, 771−776.
(31) Miyase, H.; Asai, Y.; Takano, A.; Matsushita, Y. Kaleidoscopic tiling patterns with large unit cells from ABC star-shaped terpolymer/diblock copolymer blends with hydrogen bonding interaction. *Macromolecules* **2017**, *50*, 979−986.
(32) Salim, N. V.; Hameed, N.; Hanley, T. L.; Guo, Q. P. Microphase separation induced by competitive hydrogen bonding interactions in semicrystalline triblock copolymer/homopolymer complexes. *Soft Matter* **2013**, *9*, 6176−6184.
(33) Zhang, J.; Deng, Y.; Wei, J.; Sun, Z.; Gu, D.; Bongard, H.; Liu, C.; Wu, H.; Tu, B.; Schuth, F.; Zhao, D. Design of amphiphilic ABC triblock copolymer for templating synthesis of large-pore ordered mesoporous carbons with tunable pore wall thickness. *Chem. Mater.* **2009**, *21*, 3996−4005.
(34) Qiang, Z.; Xue, J.; Stein, G. E.; Cavicchi, K. A.; Vogt, B. D. Control of ordering and structure in soft templated mesoporous carbon films by use of selective solvent additives. *Langmuir* **2013**, *29*, 8703−8712.
(35) Deng, G.; Qiang, Z.; Lecorchick, W.; Cavicchi, K. A.; Vogt, B. D. Nanoporous nonwoven fibril-like morphology by cooperative self-assembly of poly(ethylene oxide)-*block*-poly(ethyl acrylate)-*block*-polystyrene and phenolic resin. *Langmuir* **2014**, *30*, 2530−2540.
(36) Bastakoti, B. P.; Ishihara, S.; Leo, S. Y.; Ariga, K.; Wu, K. C. W.; Yamauchi, Y. Polymeric micelle assembly for preparation of large-sized mesoporous metal oxides with various compositions. *Langmuir* **2014**, *30*, 651−659.
(37) Li, Y.; Bastakoti, B. P.; Imura, M.; Hwang, S. M.; Sun, Z.; Kim, J. H.; Dou, S. X.; Yamauchi, Y. Synthesis of mesoporous TiO_2/SiO_2 hybrid films as an efficient photocatalyst by polymeric micelle assembly. *Chem. - Eur. J.* **2014**, *20*, 6027−6032.
(38) Suzuki, N.; Imura, M.; Nemoto, Y.; Jiang, X.; Yamauchi, Y. Mesoporous SiO_2 and Nb_2O_5 thin films with large spherical mesopores through self-assembly of diblock copolymers: unusual conversion to cuboidal mesopores by Nb_2O_5 crystal growth. *CrystEngComm* **2011**, *13*, 40−43.
(39) Jiang, X.; Suzuki, N.; Bastakoti, B. P.; Wu, K. C. W.; Yamauchi, Y. Synthesis of continuous mesoporous alumina films with large-sized cage-type mesopores by using diblock copolymers. *Chem. - Asian J.* **2012**, *7*, 1713−1718.
(40) Werner, J. G.; Hoheisel, T. N.; Wiesner, U. Synthesis and characterization of gyroidal mesoporous carbons and carbon monoliths with tunable ultralarge pore size. *ACS Nano* **2014**, *8*, 731−743.
(41) Liu, C. C.; Chu, W. C.; Li, J. G.; Kuo, S. W. Mediated competitive hydrogen bonding form mesoporous phenolic resins templated by poly(ethylene oxide-b-ε-caprolactone-b-l-lactide) triblock copolymers. *Macromolecules* **2014**, *47*, 6389−6400.
(42) Li, J. G.; Lin, R. B.; Kuo, S. W. Hierarchical mesoporous silica fabricated from an ABC triblock terpolymer as a single template. *Macromol. Rapid Commun.* **2012**, *33*, 678−682.
(43) Chu, W. C.; Cheng, C. C.; Bastakoti, B. P.; Kuo, S. W. Hierarchical mesoporous silicas templated by PE-b-PEO-b-PLA triblock copolymer for fluorescent drug delivery. *RSC Adv.* **2016**, *6*, 33811−33820.
(44) Hua, C.; Dong, C. M.; Wei, Y. Versatile strategy for the synthesis of dendronlike polypeptide/linear poly (ε-caprolactone)

DOI: 10.1021/acs.macromol.8b00087
Macromolecules 2018, 51, 3017−3029

block copolymers via click chemistry. *Biomacromolecules* **2009**, *10*, 1140−1148.
(45) Kotharangannagari, V. K.; Sanchez-Ferrer, A.; Ruokolainen, J.; Mezzenga, R. Photoresponsive Reversible Aggregation and Dissolution of Rod−Coil Polypeptide Diblock Copolymers. *Macromolecules* **2011**, *44*, 4569−4573.
(46) Li, P. C.; Lin, Y. C.; Chen, M.; Kuo, S. W. Self-assembled structures from PEGylated polypeptide block copolymers synthesized using a combination of ATRP, ROP, and click chemistry. *Soft Matter* **2013**, *9*, 11257−11269.
(47) Lin, Y. C.; Kuo, S. W. Hierarchical Self-Assembly of POSS-Containing Polypeptide Block Copolymers Synthesized using a Combinations of ATRP, ROP, and Click Chemistry. *Polym. Chem.* **2012**, *3*, 882−891.
(48) Coleman, M. M.; Graf, J. F.; Painter, P. C. *Specific Interactions and the Miscibility of Polymer Blends*; Technomic Publishing: Lancaster, PA, 1991.
(49) Kuo, S. W.; Lin, C. L.; Chang, F. C. Phase behavior and hydrogen bonding in ternary polymer blends of phenolic resin/poly(ethylene oxide)/poly(ε-caprolactone). *Macromolecules* **2002**, *35*, 278−285.
(50) Kuo, S. W.; Chang, F. C. The study of miscibility and hydrogen bonding in blends of phenolics with poly(ε-caprolactone). *Macromol. Chem. Phys.* **2001**, *202*, 3112−3119.
(51) Kuo, S. W.; Chen, C. J. Using hydrogen bonding interactions to control the peptide secondary structures and miscibility behavior of poly(L-glutamates)s with phenolic resin. *Macromolecules* **2011**, *44*, 7315−7326.
(52) Wan, Y.; Gan, Z.; Li, Z. Effects of the surface charge on the stability of PEG-b-PCL micelles: simulation of the interactions between charged micelles and plasma components. *Polym. Chem.* **2014**, *5*, 1720−1727.
(53) Klok, H. A.; Langenwalter, J. F.; Lecommandoux, S. Self-assembly of peptide-based diblock oligomers. *Macromolecules* **2000**, *33*, 7819−7826.
(54) Papadopoulos, P.; Floudas, G.; Klok, H. A.; Schnell, I.; Pakula, T. Self-assembly and dynamics of poly(γ-benzyl-l-glutamate) peptides. *Biomacromolecules* **2004**, *5*, 81−91.
(55) Papadopoulos, P.; Floudas, G.; Schnell, I.; Lieberwirth, I.; Nguyen, T. Q.; Klok, H. A. Thermodynamic confinement and α-helix persistence length in poly(γ-benzyl-l-glutamate)-*b*-poly(dimethyl siloxane)-*b*-poly(γ-benzyl-l-glutamate) triblock copolymers. *Biomacromolecules* **2006**, *7*, 618−626.
(56) Cai, C.; Lin, J.; Lu, Y.; Zhang, Q.; Wang, L. Polypeptide self-assemblies: nanostructures and bioapplications. *Chem. Soc. Rev.* **2016**, *45*, 5985−6012.
(57) Kuo, S. W.; Lee, H. F.; Huang, C. F.; Huang, C. J.; Chang, F. C. Synthesis and self-assembly of helical polypeptide-random coil amphiphilic diblock copolymer. *J. Polym. Sci., Part A: Polym. Chem.* **2008**, *46*, 3108−3119.
(58) Gitsas, A.; Floudas, G.; Mondeshki, M.; Spiess, H. W.; Aliferis, T.; Iatrou, H.; Hadjichristidis, N. Control of peptide secondary structure and dynamics in poly(γ-benzyl-l-glutamate)-*b*-polyalanine peptides. *Macromolecules* **2008**, *41*, 8072−8080.
(59) Kuo, S. W.; Lee, H. F.; Huang, W. J.; Jeong, K. U.; Chang, F. C. Solid state and solution self-assembly of helical polypeptides tethered to polyhedral oligomeric silsesquioxanes. *Macromolecules* **2009**, *42*, 1619−1626.
(60) Chiang, Y. W.; Hu, Y. Y.; Li, J. N.; Huang, S. H.; Kuo, S. W. Tri-layered single crystals with epitaxial growth in poly(ethylene oxide)−block−poly(ε-caprolactone)−block−poly(L-lactide) thin films. *Macromolecules* **2015**, *48*, 8526−8533.
(61) Kuo, S. W.; Chen, C. J. Functional polystyrene derivatives influence the miscibility and helical peptide secondary structures of poly(γ-benzyl l-glutamate). *Macromolecules* **2012**, *45*, 2442−2452.
(62) Bonduelle, C. Secondary structures of synthetic polypeptide polymers. *Polym. Chem.* **2018**, *9*, 1517−1529.

DOI: 10.1021/acs.macromol.8b00087
Macromolecules 2018, 51, 3017−3029